Joule Heating Effect of Buongiorno Model of Hybrid Nanofluid Flow With Homogeneous-Heterogeneous Reaction and Heat Generation/Absorption

Muhammad Jawad *, Zhuojia Fu, Waris Khan

Posted Date: 23 May 2024

doi: 10.20944/preprints202405.1553.v1

Keywords: Hybrid nanofluid flow; Darcy Forcheimer; Bongiorno Model; heat generation/absorption; thermal radiation; Homogeneous and Heterogeneous reaction

Article

Joule Heating Effect of Buongiorno Model of Hybrid Nanofluid flow with Homogeneous-Heterogeneous Reaction and Heat Generation/Absorption

Muhammad Jawad *[1], Zhuojia Fu [1] and Waris Khan [2]

[1] Center for Numerical simulation software in Engineering and Science, college of Mechanics and Material s, Hohai University, Nanjing 211100, PR China
[2] Department of Mathematics and Statistics, Hazara University Mansehra, 21120, KP, Pakistan,
* Correspondence: 20230949@hhu.edu.cn

Abstract: In this research work the study of Buongiorno Model Darcy Forchheimer flow of Hybrid nanofluid flow on isothermal permeable stretch/shrink sheet with homogeneous and heterogeneous reaction is investigated. The effects of MHD, thermal radiation, viscous dissipation, Joule heating, and heat generation/absorption are taken into account. Hybrid nanofluids can act as a medium for heterogeneous-homogeneous reactions. The nanoparticles dispersed in the fluid can influence reaction kinetics and species transport, potentially, altering reaction rates and pathways. The applications of HNF in reactions, both homogeneous and heterogeneous, lie in leveraging their enhanced thermal properties, catalytic potential, and improved mixing capabilities to optimize reaction efficiency and control reaction conditions. Similarity transformation is used to convert a set of PDEs into a set of ODEs. HAM is used for the solution of the obtained ODEs system. In a heterogeneous reaction, the concentration gradient is amplified; in a homogeneous reaction, the impact is opposite. Moreover, at higher compositions of HNPs, the concentration and velocity rise while the temperature falls. Furthermore, as the values of homogeneous and heterogeneous reactions increase, the concentration falls. It is reliable with the idea that a greater reaction rate lowers the diffusion rate. Nevertheless, these parameters do not affect temperature or velocity.

Keywords: hybrid nanofluid flow; Darcy Forcheimer; Bongiorno model; heat generation/absorption; thermal radiation; homogeneous and heterogeneous reaction

1. Introduction

A nanofluid is a fluid that has been mixed with a base fluid, like water, ethylene glycol, or oil, and contains nanoparticles, which are particles smaller than 100 nanometers. Researcher are highly interested in studying nanofluids due to their enhance thermal and physical properties compared to base fluid. Nanoparticles in nanofluids can significantly increase thermal conductivity, improve heat transfer rates, and other properties like viscosity and stability. Nanofluid have a numerous of potential uses like cooling and heat transfer, energy sector, biomedical applications, manufacturing and materials, Automotive and Transportation, renewable energy, nanofluid based sensors and devices. The new class of heat transmission fluid, known as a nanofluid, was created by suspending nanoparticles in a base fluid and was considered by Choi and Eastman [1]. Xuan et al. [2] scrutinized performance of heat transmission of NF and predicting convective heat transmission of nanofluid by single phase fluids and multiphase feature of the nanofluid. Buongiorno [3] scrutinized the impacts of thermophoresis and Brownian diffusion on the properties of NF for boundary layer flow. Dharmalingam et al. [4] described experimently and mathematically flow of NF with heat transmission. Tielke et al. [5] investigated water based nanofluid for their thermal conductivity measurements and potential applications. A novel scaled correlation to forecast the measurement of NF thermal conductivity was presented by Coccia et al. [6]. Alami et al. [7] explored the implications

 doi:10.20944/preprints202405.1553.v1

and limitations of conventional heat transmission coefficient calculation methods. Eswara et al. [8] studied bioconvection nanofluid flow on stretching porous media permeable sheet with MHD. The 2-D micropolar NF laminar incompressible flow in a steady channel with MHD was studied by Alahmadi et al. [9]. Ali et al. [10] examined 2-D NF flow with EMHD, variable heat flux, thermal radiation. The research work related to nanofluid flow has seen in [11–13].

Hybrid nanfluid are a type of nanofluid that combines nanoparticles with different types, shapes, or materials to form a synergistic mixture within a base fluid. These combinations include a mix of metallic nonmetallic, or polymeric nanoparticles. The goal is to enhance specific properties by leveraging the unique characteristics of each type of nanoparticle. Research on hybrid nanofluids is ongoing, exploring different nanoparticle combinations and base fluid to achieve enhanced heat transfer, rheological behavior, and stability. Hybrid nanofluids have a significance application in various fields like heat exchangers and cooling system, Solar thermal system, electronics and thermal management, nuclear reactors, biomedical applications, manufacturing and materials processing, automotive, aerospace, renewable energy etc. Rosca et al. [14] studied Buongiorno model of HNF flow on a permeable stretch/shrink sheet. Hayat et al. [15] investigated 3-D HNF rotating flow on stretch sheet with radiation and heat generation impacts. Boundary layer flow of HNF with heat transmission on stretch/shrink sheets was discussed by Waini et al. [16]. El-Zahar et al. [17] described thermal convective boundary condition of HNF flow through a circular cylinder with MHD impact. The uses and advantages of HNF in photovoltaic systems and solar energy were covered by Rasheed et al. [18]. waini et al. [19] explored radiated HNF flow on steady nonlinear stretch/shrink sheet. Nadeem et al. [20] scrutinized HNF flow on a convective heat permeable shrink/stretch sheet at a stagnation point with MHD impacts. MHD HNF flow on an exponential stretch/shrink surface with heat generation/apsorption was studied by Sarfaraz et al. [21] and bvp4c is used for numerical solution. The related work has been seen in [22–24].

Homogenous and heterogeneous reactions refer to different types of chemical reactions on based on the phases of the reactants involved. In homogeneous reaction, all the products and reactants are in the same phase (e.g., all liquid, all solid, or all gaseous). In a heterogeneous reaction, reactant and products are in different phases (e.g., gas reaction with a solid, liquid reacting with a gas, etc). Homogenous and heterogeneous reactions have many applications in chemistry and other related fields, some of them are catalysis, environmental science, chemical engineering, material science, biological system, etc. HNF flow at the stagnation point on a stretch/shrink sheet with heterogeneous- homogeneous reactions was described by Waini et al. [25]. Xu et al. [26] explored Buongiorno Model of NF with homogeneous - heterogeneous reaction. Alarabi et al. [27] discussed HNF flow for Darcy-Forchheimer in stretch/shrink cylinder with MHD, Joule heating, and hetrogeneous-homogeneous reaction. Ramzan et al [28] studied NF flow with MHD impacts and homogeneous and heterogeneous reaction and utilized bvp4c for numerical computation. Anuar et al. [29] explored MHD flow of HNF at a stagnation point with heterogeneous - homogeneous reaction. Bala et al [30] scrutinized Casson NF flow on an unsteady porous media stretch/shrink sheet with heat source/sink and heterogeneous-homogeneous reaction.

The branch of physics deals with the study of the behavior of electrically conducting fluids in the occurrence of magnetic fields, including salt water, liquid metals, and plasma is known as MHD. Some uses of MHD are astrophysics, fusion energy research, electric power generation, MHD propulsion, geophysics, material processing, plasma and space research, environmental science, etc. Khashi'ie et al. [31] examined HNF flow with heat transmission and Joule heating effects on a moving plate. Reddy et al. [32] scrutinized MHD effects of viscous fluid flow with heat transmission in a porous media cylinder. Abbas et al. [33] explored incompressible MHD fluid flow on steady cylinder with variable thermal conductivity. MHD 2-D Williamson HNF incompressible flow with Joule heating influence was deliberated by Rashad et al. [34]. MHD Casson NF flow on stretched surface was scrutinized by Suresh et al. [35] along with the impacts of activation energy and thermal radiation. Hybrid nanofluid obtained by adding Al_2O_3 and Cu in Base fluid as shown in Figure 1.

The following points highlight the novelty, goal, and aspects that this research communication and paper attempt to investigate:

 doi:10.20944/preprints202405.1553.v1

- The mathematical 2-D flow model of HNF over porous stretch/shrink sheet using water as the base fluid and Cu, Al_2O_3 as nanoparticles.
- This analysis investigates an appropriate interpretation of Darcy-Forchhiemer and Buongiorno models of HNF flow on stretch/shrink sheet.
- The use of significant mechanisms such as heat generation/absorption, viscous dissipation, and Joule heating effect, homogeneous and heterogeneous reaction enhances the originality of this work.
- A system of PDEs is converted into a set of ODEs using similarity variables, and then HAM is applied for the solution of the obtained ODEs.
- Tables and graphs are used to explain the results of the numerical analysis. The percentage % comparison of NF and HNF of velocity and energy are shown through graph.

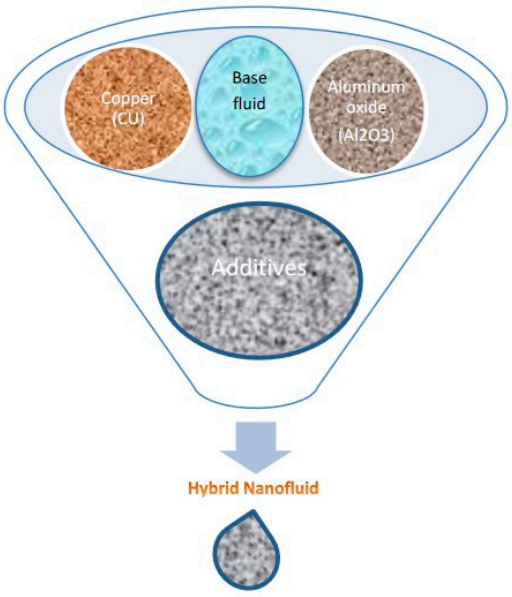

Figure 1. Hybrid Nanofluid.

2. Problem Formulation

In this study, we examine Darcy-Forchheimer MHD flow of HNF with heterogeneous-homogeneous reaction on steady stretch/shrink sheet. Velocity components in $x-$ and $y-$ directions are signified as (u,v). The plate normal coordinate is in y -direction, and stream wise flow is in $x-$ direction. It is supposed that the mass flux velocity is with v_0, $v_0 < 0$ for suction and $v_0 > 0$ for injection or withdraw of the fluid and the surface velocity is $u_w(x)$. Surface and ambient temperatures and concentrations are given as T_∞, T_w, and C_∞, C_w .

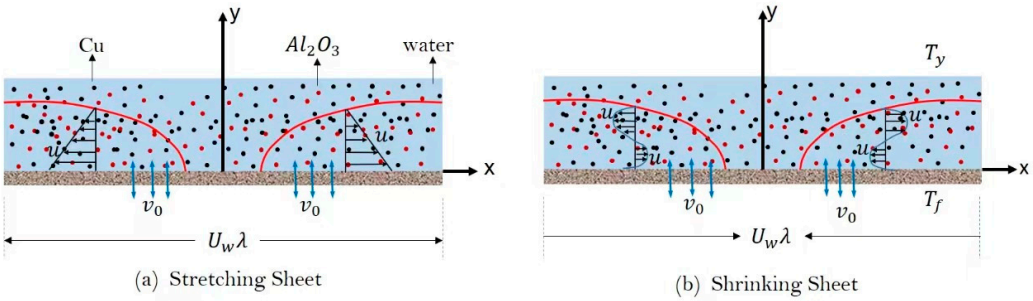

 doi:10.20944/preprints202405.1553.v1

Figure 2. Geometries of the flow problem.

Homogeneous-heterogeneous reactions can write as

$$A+2B\to 3B,\ \text{rates}=k_1ab^2 \tag{1}$$

$$A\to B,\ \text{rates}=k_s a \tag{2}$$

Where the chemical concentrations a and b for species, A,B, with rate constant k_1 and k_s. The governing equations of the flow problem are

$$\frac{\partial u}{\partial x}+\frac{\partial v}{\partial y}=0, \tag{3}$$

$$\left(u\frac{\partial}{\partial x}+v\frac{\partial}{\partial y}\right)u=\frac{\mu_{hnf}}{\rho_{hnf}}\left(\frac{\partial^2 u}{\partial y^2}\right)-\frac{\sigma_{hnf}}{\rho_{hnf}}\left(B_0^2u\right)-\frac{\nu_{hnf}}{K}u-\frac{C_b}{\sqrt{K}\rho_{hnf}}u^2, \tag{4}$$

$$\left(v\frac{\partial}{\partial y}+u\frac{\partial}{\partial x}\right)T=\frac{k_{hnf}}{\left(\rho c_p\right)_{hnf}}\left(\frac{\partial^2 T}{\partial y^2}\right)+\left(\frac{\partial u}{\partial y}\right)^2\frac{\sigma_{hnf}}{\left(\rho c_p\right)_{hnf}}$$

$$+\tau\left(D_B\frac{\partial C}{\partial y}\frac{\partial T}{\partial y}+\left(\frac{\partial T}{\partial y}\right)^2\frac{D_T}{T_\infty}\right)+\frac{\mu_{hnf}}{\left(\rho c_p\right)_{hnf}}\beta_0^2u^2+\frac{Q_0}{\left(\rho c_p\right)_{hnf}}\left(T-T_\infty\right)-\frac{1}{\left(\rho c_p\right)_{hnf}}\frac{\partial q_r}{\partial y}, \tag{5}$$

$$\left(v\frac{\partial}{\partial y}+u\frac{\partial}{\partial x}\right)C=\left(\frac{\partial^2 C}{\partial y^2}\right)D_B+\left(\frac{\partial^2 T}{\partial y^2}\right)\frac{D_T}{T_\infty}, \tag{6}$$

$$\left(u\frac{\partial}{\partial x}+v\frac{\partial}{\partial y}\right)a=D_A\left(\frac{\partial^2 a}{\partial y^2}\right)-k_1\left(ab^2\right), \tag{7}$$

$$\left(u\frac{\partial}{\partial x}+v\frac{\partial}{\partial y}\right)b=D_B\left(\frac{\partial^2 a}{\partial y^2}\right)+k_1\left(ab^2\right), \tag{8}$$

$$u=u_w\left(x\right)=U_w\left(x\right)\lambda, v=v_0, T=T_w, D_B\left(\frac{\partial C}{\partial y}\right)+\frac{D_T}{T_\infty}\left(\frac{\partial T}{\partial y}\right)=0,$$

$$D_A\left(\frac{\partial a}{\partial y}\right)=k_s\left(a\right), D_B\left(\frac{\partial b}{\partial y}\right)=-k_s\left(a\right)\ \ at\ \ y=0, \tag{9}$$

$$u=u_e\left(x\right)\to 0, C\to C_\infty, T\to T_\infty, a\to a_0, b\to 0\ \ \ at\ \ \ y\to\infty. \tag{10}$$

Where the temperature of HNF is T and C is the concentration. While, D_A, D_B are the diffusion coefficients of species A,B and $a_0>0$. Thermophoretic diffusion coefficient is D_T, $F=\dfrac{C_b}{x\sqrt{K}}$ is the inertia coefficient. Tables 1 and 2 signify the thermophysical possessions of HNF.

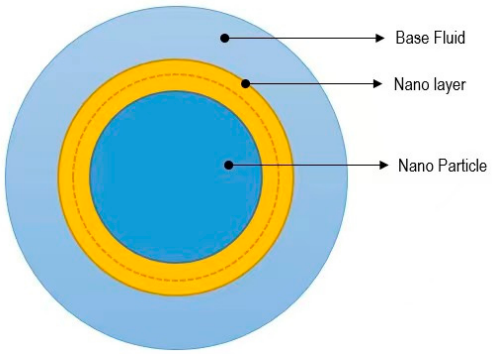

Figure 3. Nanoparticle with interfacial nanolayer structure.

 doi:10.20944/preprints202405.1553.v1

Table 1. Thermophysical properties of Cu beside with Al_2o_3 and H_2o [4].

Thermo-Physical	Cu	Al_2O_3	H_2O
$\rho(kg/m^3)$	8933	3970	9971
$k(W/mK)$	400.0	40.0	0.6130
$c_p(J/kgK)$	385.0	765.0	4179.0
$\beta\times10^5(1/K)$	1.67	0.85	21

Table 2. Illustration of the thermophysical properties of the applied model [4].

Property	Hybrid nanofluid
Thermal capacity	$(\rho c_p)_{hnf} = (\rho c_p)_f (1-\phi_{hnf}) + (\rho c_p)_{s1}\phi_1 + (\rho c_p)_{s2}\phi_2$
Viscosity	$(\mu)_{hnf} = (1-\phi_{hnf})^{-2.5}$
Thermal conductivity	$\frac{k_{hnf}}{k_f} = \left[\frac{\left(\frac{\phi_1 k_{s1}+\phi_2 k_{s2}}{\phi_{hnf}}\right) + 2k_f + 2(\phi_1 k_{s1}+\phi_2 k_{s2}) - 2\phi_{hnf}k_f}{\left(\frac{\phi_1 k_{s1}+\phi_2 k_{s2}}{\phi_{hnf}}\right) + 2k_f - 2(\phi_1 k_{s1}+\phi_2 k_{s2}) - \phi_{hnf}k_f}\right]$
Density	$\rho_{hnf} = \rho_f(1-\phi_{hnf}) + \rho_{s1}\phi_1 + \rho_{s2}\phi_2$
Electrical Conductivity	$\frac{\sigma_{hnf}}{\sigma_{nf}} = \left[\frac{\sigma_2(1+2\phi_2)+\sigma_{nf}(1-2\phi_2)}{\sigma_2(1-\phi_2)+\sigma_{nf}(1+\phi_2)}\right]$, $\frac{\sigma_{nf}}{\sigma_{bf}} = \left[\frac{(1+2\phi_3)\sigma_3+(1-2\phi_3)\sigma_{bf}}{(1-\phi_3)\sigma_3+(1+\phi_3)\sigma_{bf}}\right]$

 doi:10.20944/preprints202405.1553.v1

Specific heat capacity of HNF is $\left(\rho c_p\right)_{hnf}$, density of HNF is ρ_{hnf}, density of base fluid is ρ_f, dynamic viscosity of HNF is μ_{hnf}, electrical conductivity of base fluid is σ, υ_f is the kinematic viscosity of base fluid and electrical conductivity of HNF is σ_{hnf}. k_{hnf}, k_f is the thermal conductivity of HNF and base fluid. Nanoparticle's volume frictions are $\phi_1\left(Al_2O_3\right), \phi_2\left(Cu\right)$.

Figure 4. Copper $\left(Cu\right)$ has various uses.

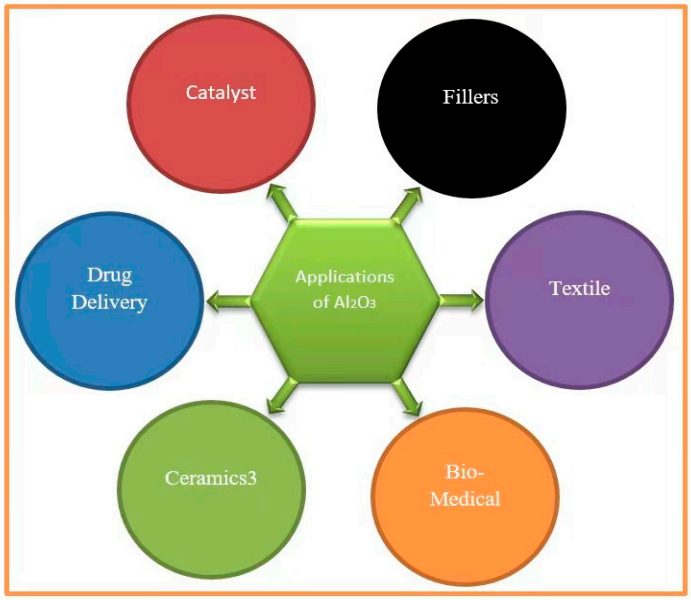

Figure 5. Applications of Al_2O_3 nanoparticle.

 doi:10.20944/preprints202405.1553.v1

Similarity transformations are;

$$\eta = y\left(\frac{a}{\nu_f}\right)^{1/2}, v = -\left(\nu_f a\right)^{1/2} f(\eta), u = axf'(\eta), \Phi = \frac{C - C_\infty}{C_w - C_\infty},$$
$$\theta = \frac{T - T_\infty}{T_w - T_\infty}, a = a_0 g(\eta), b = a_0 h(\eta), v_0 = -\left(\nu_f a\right)^{1/2} S \quad (11)$$

By using the equ (11) in equs (3-10), equ(3) is identically proved, other equations are gotten as;

$$f'''\left(\frac{\mu_{hnf}/\mu_f}{\rho_{hnf}/\rho_f}\right) - f'^2 + ff'' - Mf'\left(\frac{\sigma_{hnf}/\sigma_f}{\rho_{hnf}/\rho_f}\right) - \left(\frac{\nu_{hnf}}{\nu_f}\right)k_1 f' - \left(\frac{\rho_f}{\rho_{hnf}}F_1\right)(f')^2 = 0, \quad (12)$$

$$\frac{1}{\left(\rho c_p\right)_{hnf}/\left(\rho c_p\right)_f}\left(k_{hnf}/k_f + \frac{4}{3}Rd\right)\theta'' + \frac{\frac{\mu_{hnf}}{\mu_f}}{\frac{\left(\rho c_p\right)_{hnf}}{\left(\rho c_p\right)}}Ecf''^2 + \left(N_b\theta'\Phi' + N_t\theta'^2\right)$$

$$+\frac{\frac{\sigma_{hnf}}{\sigma_f}}{\frac{\left(\rho c_p\right)_{hnf}}{\left(\rho c_p\right)}}EcMf'^2 + \Pr f\theta' + \frac{1}{\left(\rho c_p\right)_{hnf}/\left(\rho c_p\right)_f}Q_1\theta = 0, \quad (13)$$

$$\Phi'' + Scf\Phi' + \frac{N_t}{N_b}\Theta'' = 0, \quad (14)$$

$$\frac{1}{Sc}\left(g''\right) + g'f - Kh^2 g = 0, \quad (15)$$

$$\frac{1}{Sc}\left(h''\right) + h'f + Kh^2 g = 0, \quad (16)$$

$$f'(0) = \lambda, \theta(0) = 1, f(0) = S, N_t\left(\theta'(0)\right) + N_b\left(\Phi'(0)\right) = 0,$$
$$\delta h'(0) = K_s\left(g(0)\right), g'(0) = K_s\left(g(0)\right), \quad (17)$$
$$f''(\infty) \to 1, \theta(\infty) \to 0, \Phi(\infty) \to 0, h(\infty) \to 0, g(\infty) \to 1.$$

 doi:10.20944/preprints202405.1553.v1

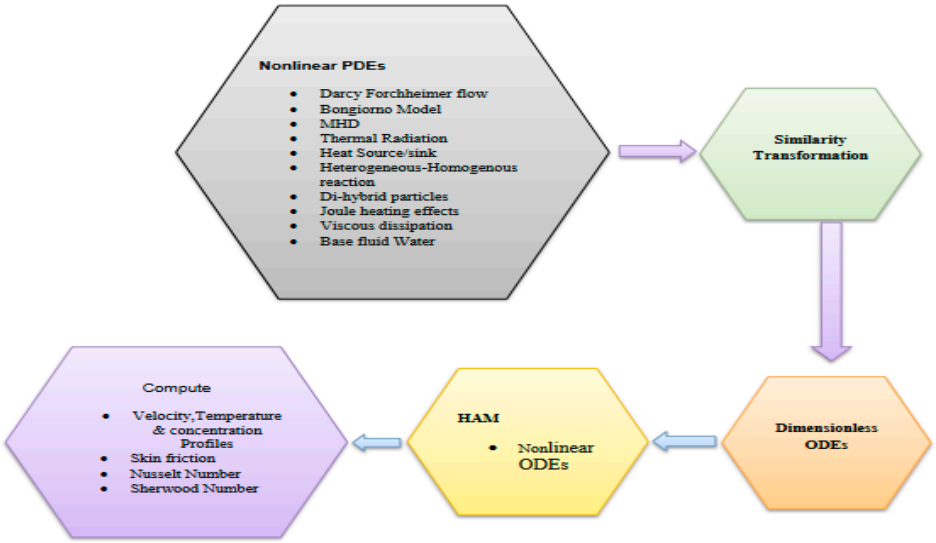

Figure 6. Block diagram of Homotopy Analysis Method.

Where Schmidt number $Sc=\frac{\nu_f}{D_B}$, permeability parameter $k_1=\frac{\mu_f}{\rho_f Ka}$, magnetic field parameter $M=\frac{\sigma\beta_0^2}{\rho_f a}, F_1=\frac{C_b}{\rho_f\sqrt{K}}$ is interial parameter, $N_T=\frac{\tau D_T\left(T_w-T_\infty\right)}{T_\infty \upsilon_f}$ is thermophoresis parameter, $Rd=\frac{4\sigma^* T_\infty^3}{k^* k_f}$ is the thermal radiation , $N_b=\frac{\tau D_B\left(C_w-C_\infty\right)}{\upsilon_f}$ is Brownian motion parameter, $\delta=\frac{D_B}{D_A}$ is the ratio of diffusion coefficient, $K=\frac{k_1 a_0^2}{c}$ is the strength of homogeneous, $Ec=\frac{u_w^2}{c_p\left(T_w-T_\infty\right)}$ is Eckert number, $\Pr=\frac{\mu c_p}{k_f}$ is the Prandtl number , $K_s=\frac{k_s}{D_A\sqrt{\frac{c}{\upsilon_f}}}$ is the strength of heterogeneous. Skin friction, Sherwood number, and Nusselt number are

$$C_f=\frac{t_w}{\mu_f u_e^2}, Sh=\frac{xq_m}{D_B\left(C_w-C_\infty\right)}, Nu=\frac{xq_w}{k_f\left(T_w-T_\infty\right)} \tag{18}$$

Where

$$t_w=-\mu_{hnf}\left(\left(u_y\right)_{y=0}\right), q_m=-D_B\left(C_y\right)_{y=0}, q_w=-k_{hnf}\left(\left(T_y\right)_{y=0}\right)+\left(q_r\right)_{y=0} \tag{19}$$

In Non-dimensional form, C_f, Nu, and Sh are written as

$$C_f Re_x^{0.5}=\frac{\mu_{hnf}}{\mu_f}f''(0),\quad NuRe_x^{-0.5}=-\left(\frac{k_{nf}}{k_f}+\frac{4}{3}Rd\right)\theta'(0), \tag{20}$$

$$Re_x^{-0.5}Sh=-\Phi'(0)$$

 doi:10.20944/preprints202405.1553.v1

3. HAM Solution

HAM is used for finding the solution of equs (12-16) with BCs (17). Mathematica software is used for this purpose. The initial guesses are taken as:

$$f_0(\eta)=1-e^{-\eta},\theta_0(\eta)=e^{-\eta},\Phi_0(\eta)=e^{-\eta},g_0(\eta)=e^{-\eta},h_0(\eta)=e^{-\eta} \tag{21}$$

The linear operators are discoursed as:

$$L_{\hat{f}}(\hat{f})=\hat{f}'''-\hat{f}',L_{\hat{\theta}}(\hat{\theta})=\hat{\theta}''-\hat{\theta},\ L_{\hat{\Phi}}(\hat{\Phi})=\hat{\Phi}''-\hat{\Phi},$$
$$\mathrm{L}_{\hat{h}}\left(\hat{h}\right)=\hat{h}''-\hat{h},\mathrm{L}_{\hat{g}}\left(\hat{g}\right)=\hat{g}''-\hat{g}, \tag{22}$$

With properties

$$L_{\hat{f}}(\gamma_1+\gamma_2e^{-\eta}+\gamma_3e^{\eta})=0,L_{\hat{\Phi}}(\gamma_6e^{-\eta}+\gamma_7e^{\eta})=0,L_{\hat{\theta}}(\gamma_4e^{-\eta}+\gamma_5e^{\eta})=0,$$
$$L_{\hat{g}}(\gamma_8e^{-\eta}+\gamma_9e^{\eta})=0,L_{\hat{h}}(\gamma_{10}e^{-\eta}+\gamma_{11}e^{\eta})=0, \tag{23}$$

Where $\gamma_i\left(i=1-11\right)$ are constants.

The zero-order deformations are:

$$(1-\zeta)L_{\hat{f}}\left[\hat{f}(\eta;\zeta)-\hat{f}_0(\eta)\right]=p\hbar_{\hat{f}}\mathrm{N}_{\hat{f}}\left[\hat{f}(\eta;\zeta)\right] \tag{24}$$

$$(1-\zeta)\ L_{\hat{\theta}}\left[\hat{\theta}(\eta;\zeta)-\hat{\theta}_0(\eta)\right]=p\hbar_{\hat{\theta}}\mathrm{N}_{\hat{\theta}}\left[\hat{\theta}(\eta;\zeta),\hat{f}(\eta;\zeta)\right] \tag{25}$$

$$(1-\zeta)\ L_{\hat{\Phi}}\left[\hat{\Phi}(\eta;\zeta)-\hat{\Phi}_0(\eta)\right]=p\hbar_{\hat{\Phi}}\mathrm{N}_{\hat{\Phi}}\left[\hat{\Phi}(\eta;\zeta),\hat{f}(\eta;\zeta),\hat{\theta}(\eta;\zeta)\right] \tag{26}$$

$$(1-\zeta)\ L_{\hat{g}}\left[\hat{g}(\eta;\zeta)-\hat{g}_0(\eta)\right]=p\hbar_{\hat{g}}\mathrm{N}_{\hat{g}}\left[\hat{g}(\eta;\zeta),\hat{f}(\eta;\zeta),\hat{h}(\eta;\zeta)\right] \tag{27}$$

$$(1-\zeta)\ L_{\hat{h}}\left[\hat{h}(\eta;\zeta)-\hat{h}_0(\eta)\right]=p\hbar_{\hat{\theta}}\mathrm{N}_{\hat{\theta}}\left[\hat{h}(\eta;\zeta),\hat{f}(\eta;\zeta),\hat{\mathrm{g}}(\eta;\zeta)\right] \tag{28}$$

Here ζ is the embedding parameter, and the non-zero auxiliary parameters are, $\hbar_{\hat{\theta}}$, $\hbar_{\hat{\Phi}}$ and $\hbar_{\hat{g}},\hbar_{\hat{h}}$. $N_{\hat{f}}$, $N_{\hat{\theta}}$, $N_{\hat{g}}$, $N_{\hat{h}}$ and $N_{\hat{\Phi}}$ are the nonlinear operators which are defined as:

$$\mathrm{N}_{\hat{f}}\left[\hat{f}(\eta;\zeta)\right]=\frac{\mu_{hnf}/\mu_f}{\rho_{hnf}/\rho_f}\hat{f}_{\eta\eta\eta}-\left(\hat{f}_\eta\right)^2+\hat{f}\hat{f}_{\eta\eta}-\left(\frac{\sigma_{hnf}/\sigma_f}{\rho_{hnf}/\rho_f}\right)M\hat{f}_\eta$$
$$-\frac{\nu_{hnf}}{\nu_f}k_1\hat{f}_\eta-\frac{\rho_f}{\rho_{hnf}}F_1\left(\hat{f}_\eta\right)^2, \tag{29}$$

$$\mathrm{N}_{\hat{\theta}}\left[\hat{f}(\eta;\zeta),\hat{\theta}(\eta;\zeta),\hat{\Phi}(\eta;\zeta)\right]=\frac{1}{\left(\rho c_p\right)_{hnf}/\left(\rho c_p\right)_f}\left(k_{hnf}/k_f+\frac{4}{3}Rd\right)\hat{\theta}_{\eta\eta}$$
$$+\frac{\frac{\mu_{hnf}}{\mu_f}}{\frac{\left(\rho c_p\right)_{hnf}}{\left(\rho c_p\right)}}Ec\hat{f}_{\eta\eta}^2+\left(N_b\hat{\theta}_\eta\hat{\Phi}_\eta+N_t\hat{\theta}_\eta^{\ 2}\right) \tag{30}$$
$$+\frac{\frac{\sigma_{hnf}}{\sigma_f}}{\frac{\left(\rho c_p\right)_{hnf}}{\left(\rho c_p\right)}}EcMf'^2+\mathrm{Pr}\,\hat{f}\hat{\theta}_\eta+\frac{1}{\left(\rho c_p\right)_{hnf}/\left(\rho c_p\right)_f}Q_1\hat{\theta}$$

 doi:10.20944/preprints202405.1553.v1

$$\mathrm{N}_{\hat{\Phi}}\left[\hat{\Phi}(\eta;\zeta),\hat{f}(\eta;\zeta),\hat{\theta}(\eta;\zeta)\right]=\hat{\Phi}_{\eta\eta}+Sc\hat{f}\hat{\Phi}+\frac{N_t}{N_b}Sc\left(n+1\right)\hat{f}\hat{\theta}_{\eta\eta},$$

(31)

$$\mathrm{N}_{\hat{g}}\left[\hat{f}(\eta;\zeta),\hat{g}(\eta;\zeta),\hat{h}(\eta;\zeta)\right]=\left(\hat{g}_{\eta\eta}\right)\frac{1}{Sc}+\hat{f}\hat{g}_{\eta}-K\hat{h}^{2}\hat{g}, \quad (32)$$

$$\mathrm{N}_{\hat{h}}\left[\hat{f}(\eta;\zeta),\hat{g}(\eta;\zeta),\hat{h}(\eta;\zeta)\right]=\frac{1}{Sc}\left(\hat{h}_{\eta\eta}\right)+\hat{h}_{\eta}\hat{f}+K\hat{h}^{2}\hat{g}, \quad (33)$$

$$\hat{f}_{\eta}\left(0,\zeta\right)=\lambda,\hat{f}\left(0,\zeta\right)=S,N_t\hat{\theta}\left(0,\zeta\right)+N_b\hat{\Phi}\left(0,\zeta\right)=0,\hat{\theta}\left(0,\zeta\right)=1,$$

$$\delta\hat{h}_{\eta}\left(0,\zeta\right)=K_s\hat{g}\left(0,\zeta\right),\hat{g}_{\eta}\left(0,\zeta\right)=K_s\hat{g}\left(0,\zeta\right), \quad (34)$$

$$\hat{f}_{\eta\eta}\left(\infty,\zeta\right)=1,\hat{\Phi}\left(\infty,\zeta\right)=0,\hat{\theta}\left(\infty,\zeta\right)=0,\hat{h}\left(\infty,\zeta\right)=0,\hat{g}\left(\infty,\zeta\right)=1.$$

4. Result and discussion

In this section we explain in Figures 7–24 the impacts of different parameters like, $M,F_1,k_1,\mathrm{Pr},Rd,N_b,Sc,N_t,K_s,K,$ on $f',\theta,\Phi,g,\mathrm{C}_f,Nu$ & Sh. The influence of growing the M on f' is shown in Figure 7 It has now been extensively established that M reduces velocity by creating drag force, which opposes the fluid's motion. Transfer phenomena are resisted by the M. This is because, due to the M, changes in the M also cause changes in the Lorentz force, which increases resistance to transportation events. Under all conditions, f' decline at a significant distance from the Stretch/shrink surface. Figure 8 shows the effect of the M on θ. When perceived in Figure 8, the thickness of the thermal BL raises as M is improved.

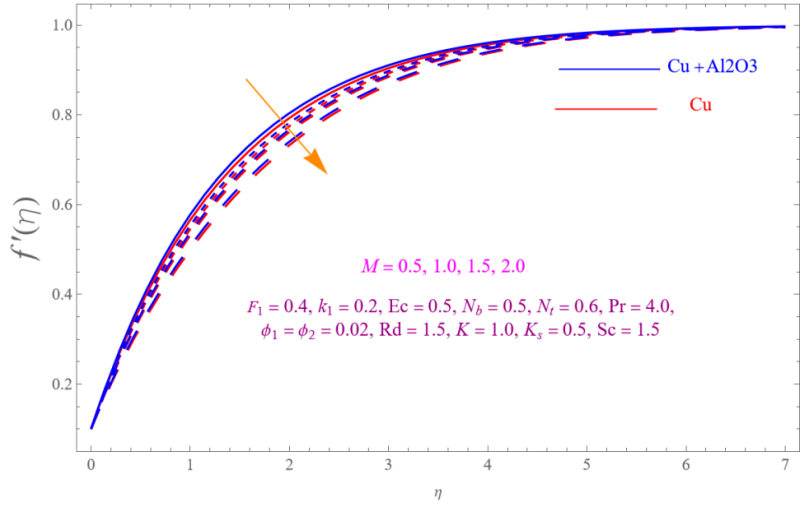

Figure 7. Effect of M on $f'(\eta)$.

Preprints.org (www.preprints.org) | NOT PEER-REVIEWED | Posted: 23 May 2024 doi:10.20944/preprints202405.1553.v1

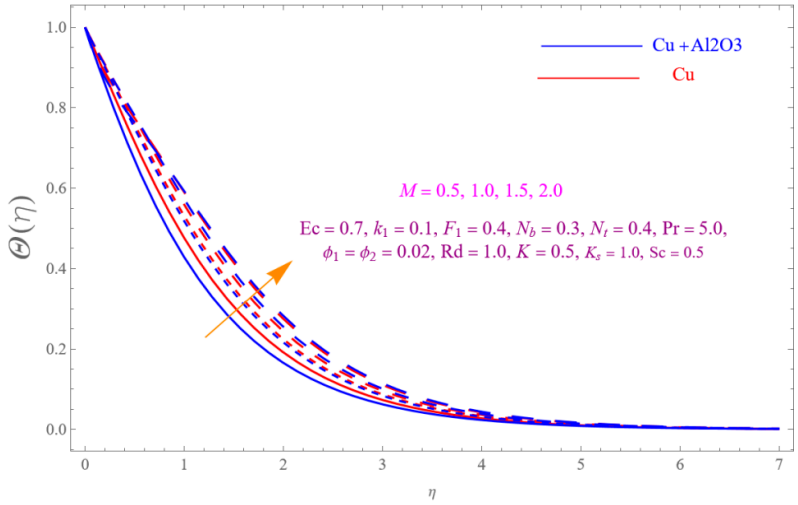

Figure 8. Effect of M on $\theta(\eta)$.

The effects of k_1 on f' are shown in Figure 9. It is evident that the presence of porous medium consequences is augmented fluid flow restriction, instigation it to move more and more slightly, which therefore decline f'. So, the impedance to fluid motion enlargements as k_1 augments. Then, the temperature rises as a consequence of a decline in f'. Thus, it can be discussed that upsurge in k_1 lessens the thickness of the BL, subsequent in an upsurge in the rate of heat transmission. The influence F_1 on f' is shown in Figure 10. When F_1 is increased, the velocity of HNF is increased, this is because the increment in F_1 produced inertial drag force, which is a barrier to f'.

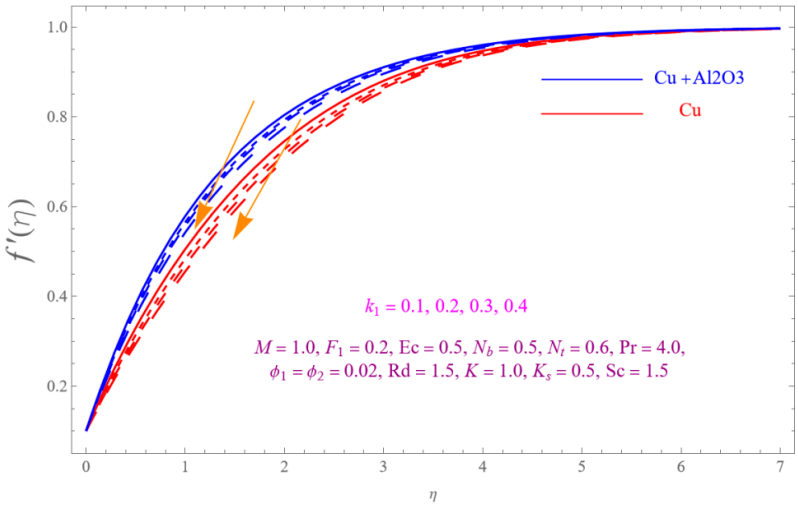

Figure 9. Influence of k_1 on $f'(\eta)$.

 doi:10.20944/preprints202405.1553.v1

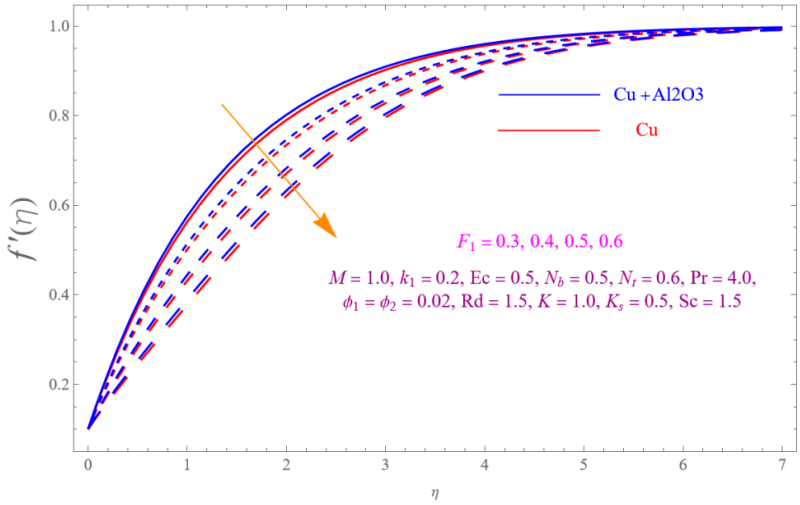

Figure 10. Influence of F_1 on $f'(\eta)$.

The impact of $\Pr$ on θ is scrutinized in Figure 11. Augmentation in $\Pr$ in declined in the thermal BL, which outcomes in reduction in θ. When $\Pr$ is augmented, υ_{nf} becomes larger than density, creating an opposing force against the fluid flow. For dissimilar values of Ec for stretch /Shrink surface the feature of θ is show in Figure 12. With the augmentation of Ec, the θ is upsurges as shown in Figure 7. Here it is noted that Ec confines the fluid motion and $Ec = 0$ signifies no viscous dissipation. The cause behind is Ec means it is the ratio of the square of the velocity of fluid far away from the surface of the boundary to the product of the specific heat at constant temperature. In case of $Ec > 0$, so that the thermal BL upsurges.

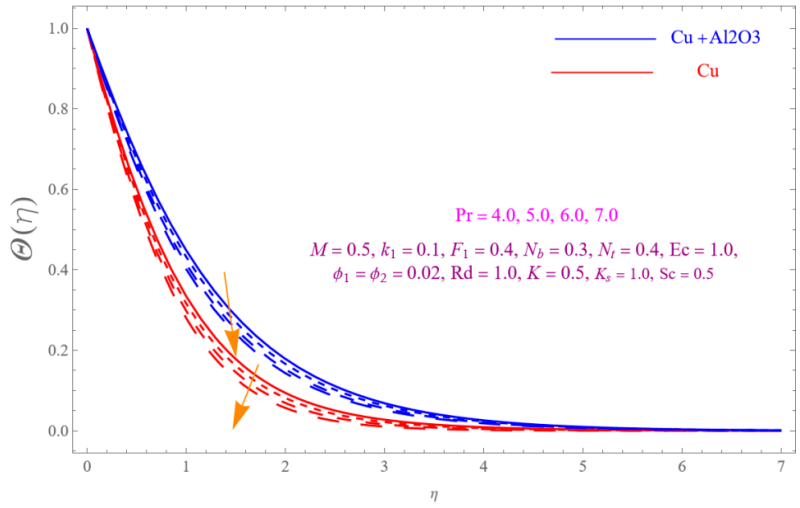

Figure 11. Effect of $\Pr$ on $\theta(\eta)$.

 doi:10.20944/preprints202405.1553.v1

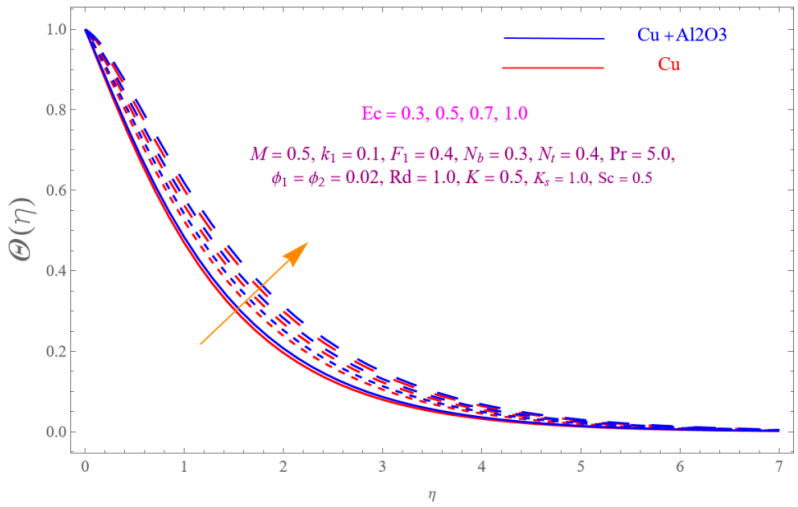

Figure 12. Influence of Ec on $\theta(\eta)$.

The increment in θ for growing in Rd can be detected in Figure 13. The Rd describes the rate at which conduction heat transmission to thermal radiation transmission occurs. Rd augments heat transmission because the augmentation in Rd will rise the thickness of the boundary layer. The thickness of the thermal boundary layer and θ increased when Rd is increased, which supplying more heat to HNF flow.

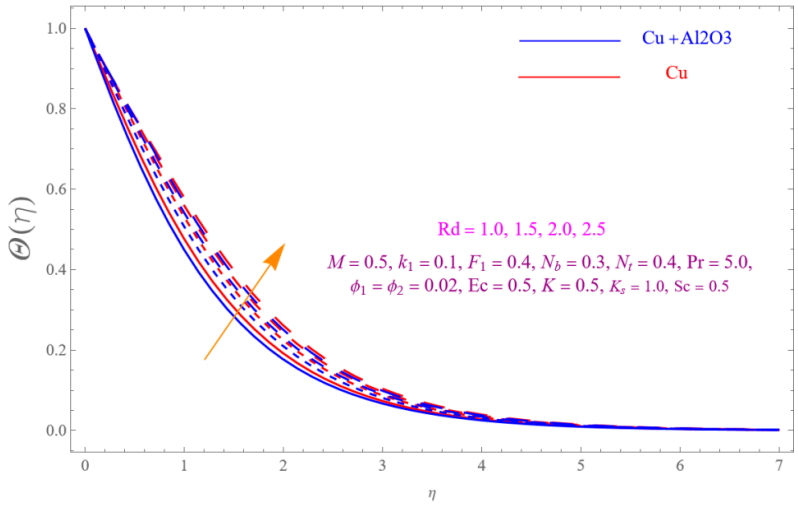

Figure 13. Effect of Rd on $\theta(\eta)$.

The behavior of the Sc in mass species is depicted in Figure 14. When Sc was inclined, the particle concentration dropped. Physically, Sc is the ratio of mass diffusivity to kinematic viscosity. The kinematic viscosity of fluid particles is skewed in relation to the influence of Schmidt number due to their physical characteristics. On the other hand, mass diffusivity decreases with Sc variation. In comparison to the Schmidt number role, concentration layers have a decreasing function.

 doi:10.20944/preprints202405.1553.v1

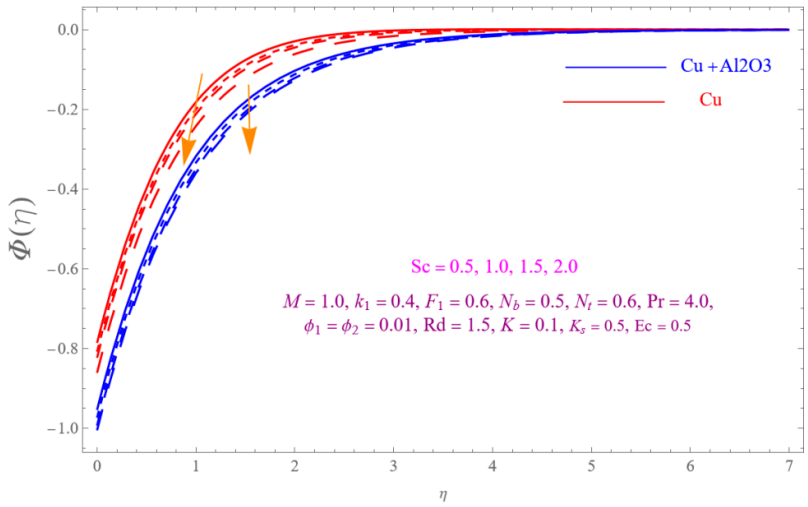

Figure 14. Influence of Sc on $\Phi(\eta)$.

The effects K and K_s on $g(\eta)$ are shown on Figure 15& Figure 16. The declining pattern of $g(\eta)$ of HNF is perceived. It is reliable with the fact that the reaction rate rises as the values of K and K_s rise, which reason the lessening in diffusion rate.

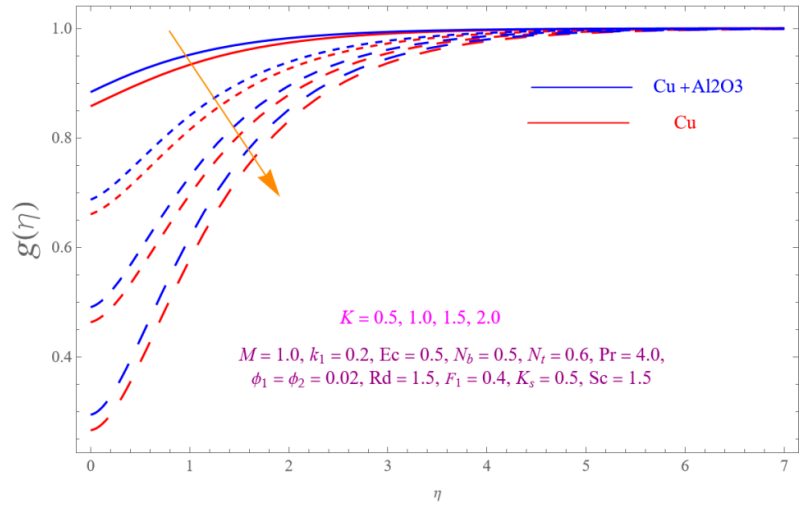

Figure 15. Effect of K on $g(\eta)$.

Preprints.org (www.preprints.org) | NOT PEER-REVIEWED | Posted: 23 May 2024 doi:10.20944/preprints202405.1553.v1

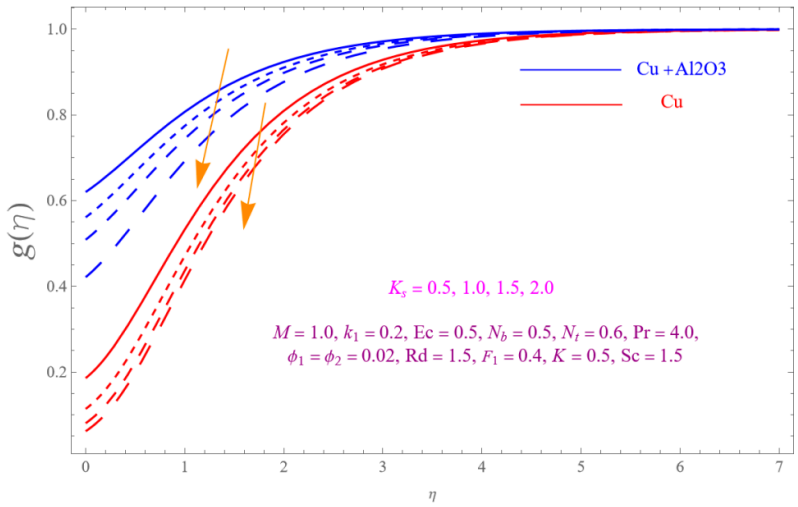

Figure 16. Influence of K on $g(\eta)$.

Furthermore, the effects are shown in Figures (17, 18), which displays that both $f''(0)$ and $\theta'(0)$ are the growing functions of M. Physically, rise in M as a result in an increasing in Lorentz force. Lorentz force creates retardation force in fluid particles. So this decelerate force slows down flow of HNF and rises in both $f''(0)$ and $\theta'(0)$.

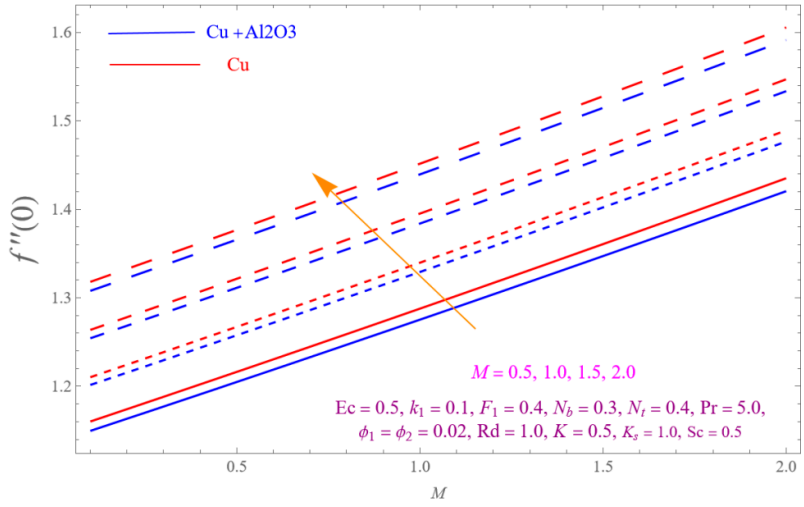

Figure 17. Impact of M on $f''(0)$.

 doi:10.20944/preprints202405.1553.v1

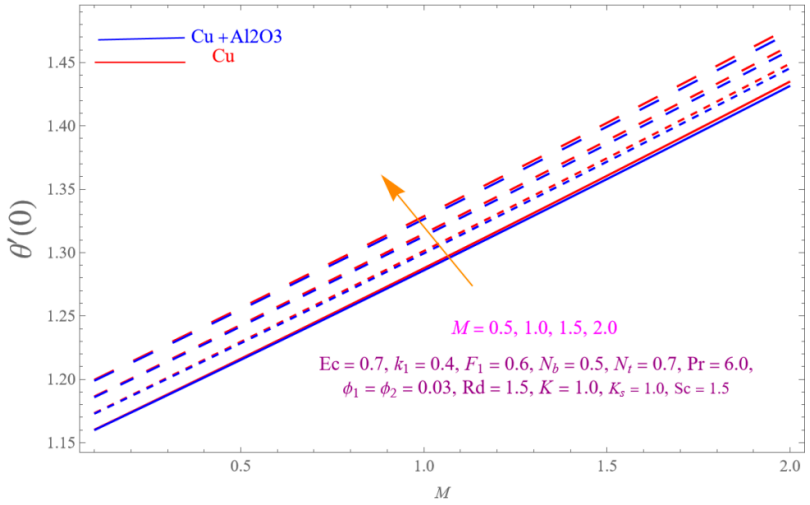

Figure 18. Effect of M on $\theta'(0)$.

Figures 13 and 14 displays the influences of k_1 and F_1 on $f''(0)$. When growing occur in k_1 and F_1 $f''(0)$ of HNF is augmented.

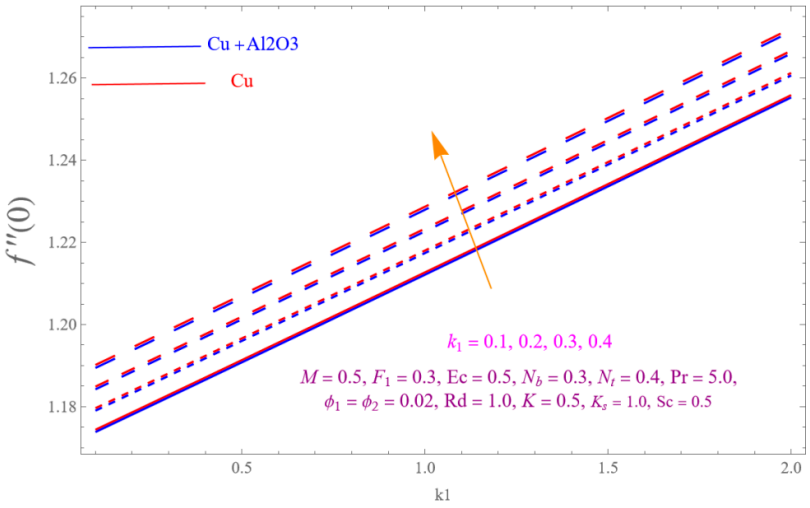

Figure 19. Influence of k_1 on $f''(0)$.

 doi:10.20944/preprints202405.1553.v1

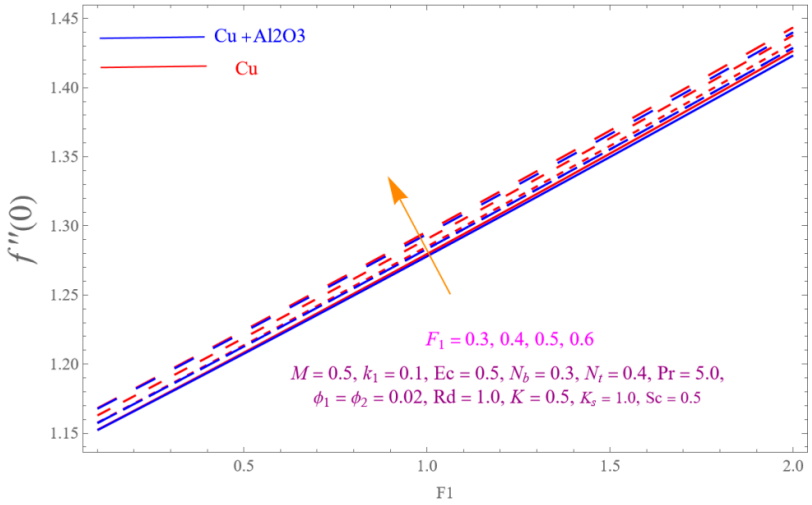

Figure 20. Effect of F_1 on $f''(0)$.

Figures 21 and 22 are drawn to scrutinize the incentive of N_t and N_b on $\theta'(0)$. The reverse effect is detected for upsurge in N_t and N_b. Base fluids with higher nanoparticle concentrations exhibit improved thermal physical properties. The concentration of additional nanoparticles within the base fluid rises with their addition, increasing the likelihood of an intermolecular collision and raising K.E raised the temperature. As a result, HNF experiences an increase in $\theta'(0)$. Also, an upsurge in N_b caused the movements of nanoparticles to shift from lower to higher concentrated regions. Figures 23 and 24 shows the reverse impact of N_t and N_b on $\Phi(0)$. Figure 25 (a, b) shows the percentage comparison of NF and HNF of velocity and energy.

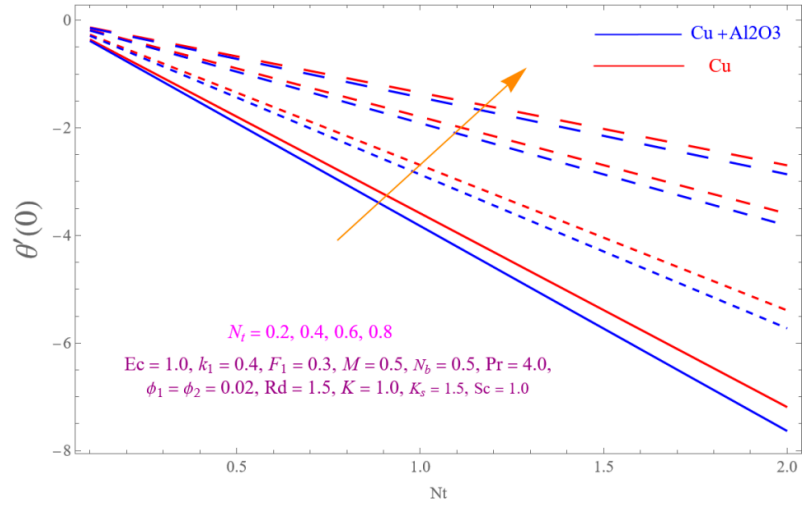

Figure 21. Impact of N_t on $\theta'(0)$.

Preprints.org (www.preprints.org) | NOT PEER-REVIEWED | Posted: 23 May 2024 doi:10.20944/preprints202405.1553.v1

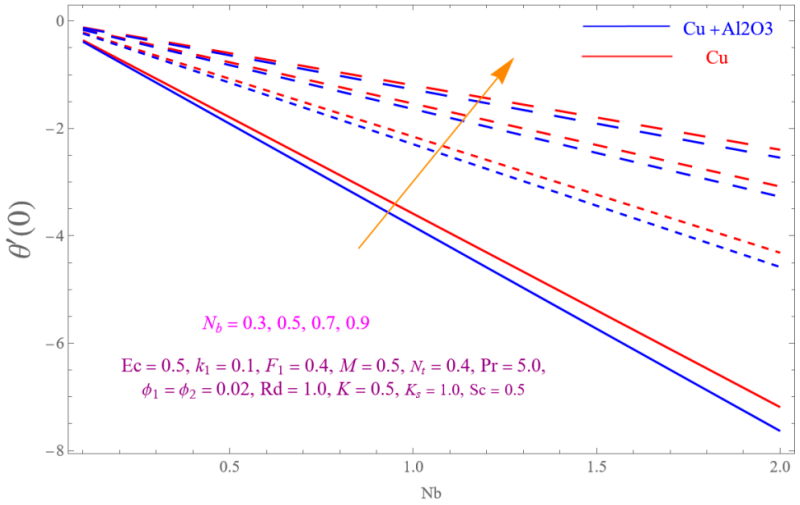

Figure 22. Effect of N_b on $\theta'(0)$.

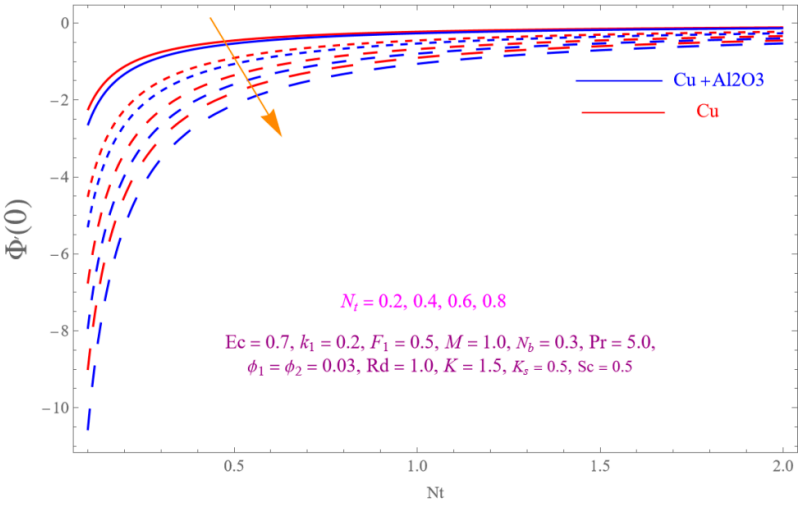

Figure 23. Effect of N_t on $\Phi'(0)$.

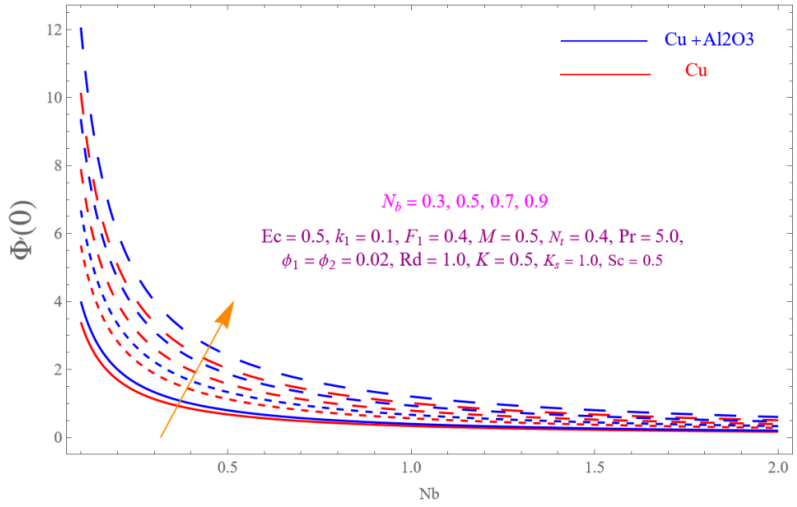

Figure 24. Influence of N_b on $\Phi'(0)$.

Preprints.org (www.preprints.org) | NOT PEER-REVIEWED | Posted: 23 May 2024 doi:10.20944/preprints202405.1553.v1

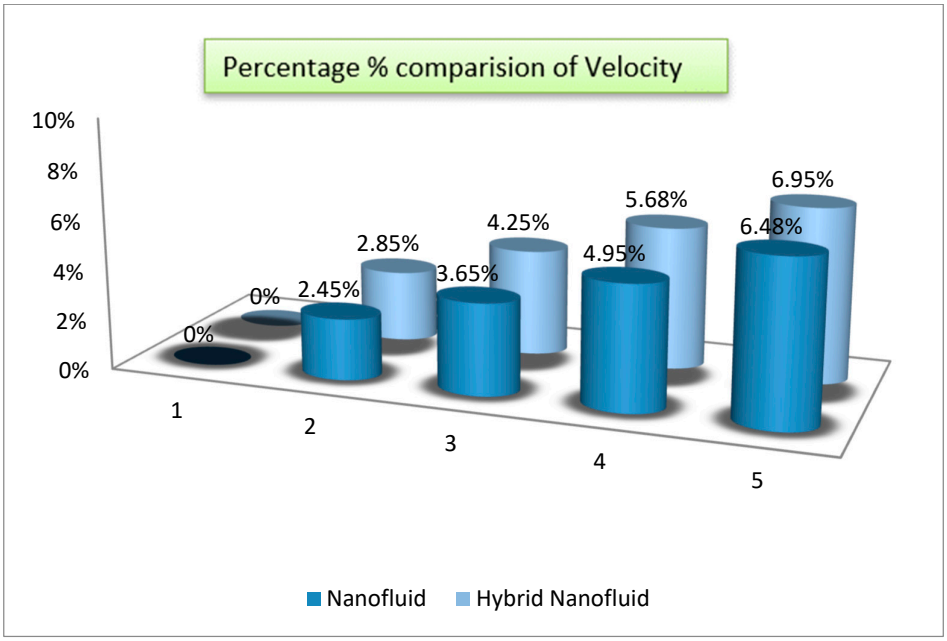

Figure 25a. The percentage comparison of NF and HNF of velocity.

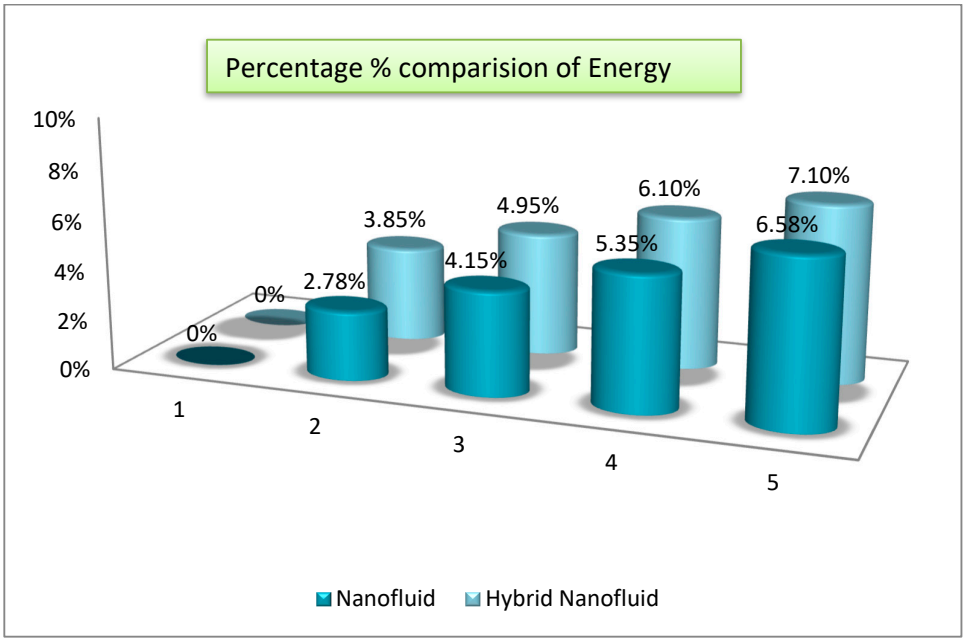

Figure 25b: The percentage comparison of NF and HNF of energy.

5. Table Discussion

The impacts of $F_1, k_1, M, \Pr, N_b, N_t, Rd, Ec, \phi_1, \phi_2$ on C_f & Nu are presented in Table 3. Growing in F_1, k_1, M , C_f is increased. The impacts of $\Pr, Ec, Rd, M, \phi_1, \phi_2, \mathrm{N}_b, N_t$ on Nu are presented in Table 3. Nusselt number is augmented when the values of $Ec, N_t, M, \phi_1, \phi_2$ is enlarged, while decline for increasing in $\Pr, N_b$. The impacts of $Sc, N_b, N_t, \phi_1, \phi_2$ on Sh are presented in Table 4. Sherwood number is increased for increasing in Sc, N_t, ϕ_1, ϕ_2 and decline for increasing in N_b .

 doi:10.20944/preprints202405.1553.v1

Table 3. Effect of different physical parameters on $C_f Re_x^{0.5} = \frac{\mu_{hnf}}{\mu_f} f''(0)$ and $NuRe_x^{-0.5} = -\left(\frac{k_{nf}}{k_f} + \frac{4}{3}Rd\right)\theta'(0)$.

F_1	k_1	M	Pr	N_b	N_t	Rd	Ec	Φ_1	Φ_2	$C_f Re_x^{0.5} = \frac{\mu_{hnf}}{\mu_f} f''(0)$	$NuRe_x^{-0.5} = -\left(\frac{k_{nf}}{k_f} + \frac{4}{3}Rd\right)\theta'(0)$
0.3	0.1	0.5	4.0	0.3	0.2	1.0	0.3	00.01	00.01	*1.18286*	.....
0.4										*1.19689*	.....
0.5										*1.21097*	.....
	0.1									*0.65218*	.....
	0.2									*1.20671*	.....
	0.3									*1.21097*	.....
		0.5								*1.21628*	*2.09861*
		1.0								*1.22959*	*2.08983*
		1.5								*1.24296*	*2.06801*
			4.0							.....	*1.70903*
			5.0							.....	*1.77541*
			6.0							.....	*1.84242*
				0.3						.....	*1.20262*
				0.5						.....	*1.21729*
				0.7						.....	*1.18071*
					0.2					.....	*1.16718*
					0.4					.....	*1.14506*
					0.6					.....	*1.14625*
						1.0				.....	*7.19478*
						1.5				.....	*5.22517*
						2.0				.....	*3.59501*
							0.3			.....	*1.19957*
							0.5			.....	*1.87312*
							0.7			.....	*1.83143*
								0.01		.....	*3.67666*
								0.02		.....	*3.66979*
								0.03		.....	*3.59314*
									0.01	.....	*3.72298*
									0.02	.....	*3.69162*
									0.03	.....	*3.73014*

Table 4. Effect of different physical parameters on $Re_x^{-0.5} Sh = -\Phi'(0)$.

Sc	N_b	N_t	Φ_1	Φ_2	$Re_x^{-0.5} Sh = -\Phi'(0)$
0.5	0.3	0.2	0.01	0.01	*2.22033*
1.0					*2.17707*
1.5					*2.13709*
	0.3				*1.07825*
	0.5				*1.01524*
	0.7				*0.63613*

 doi:10.20944/preprints202405.1553.v1

0.2			*0.39723*
0.4			*0.57299*
0.6			*1.25202*
	0.01		*2.11698*
	0.02		*2.11657*
	0.03		*2.11489*
		0.01	*2.11783*
		0.02	*2.11695*
		0.03	*2.11826*

6. Conclusions

In this research work we examine homogenous and heterogeneous reaction of Bongiorno model Darcy-Forchheimer MhD HNF flow through stretching /shrinking sheet with the impact heat viscous dissipation, thermal radiation, generation/absorption, Joule heating effect. The system of ODEs is derived from the set of PDEs by applying the proper transformations for similarity variables. The obtained ODEs is then solved by using HAM on mathematica software. The concluding remarks are obtained from the study are follows

- The f' is a declining function of k_1, M, F_1.
- Increasing in $M, Rd, Ec, \theta(\eta)$ is decreased.
- Augmenting in Sc decline the $\Phi(\eta)$.
- The decreasing pattern of $g(\eta)$ is observed for increasing in K, K_s.
- C_f is the growing function of k_1, F_1.
- Nu and C_f is the growing function of M.
- The reverse impact is observed for Nu and Sh, while increasing in N_b, N_t.

Declaration of Interest: The authors declare that they have no known competing financial interests or personal relationships that could have appeared to influence the work reported.

Competing interests: The authors declare no competing interests.

Nomenclature

$u_w(x)$	Surface velocity (m/s)	$v_0 > 0$	For injection
T_∞	Ambient temperature (K)	(u, v)	Velocity components in $x-$ and $y-$ directions. (m/s)
$v_0 < 0$	For suction	v_0	Mass flux velocity
ρ_f	Density of base fluid $\left(kgm^{-3}\right)$	C_∞	Ambient concentration
μ_{hnf}	Dynamic viscosity of HNF $\left(kgm^{-1}s^{-1}\right)$	k_1, k_s	Rate constant
a, b	Chemical concentration	T	Temperature (K)
D_A, D_B	Diffusion coefficients of species A, B	D_T	Thermophoretic diffusion
F	Inertia coefficient	C_w	Surface concentration
$(\rho c_p)_{hnf}$	Specific heat capacity of HNF $\left(m^2 s^{-2} K^{-1}\right)$	σ_{hnf}	Electrical conductivity of HNF (S/m)

 doi:10.20944/preprints202405.1553.v1

T_w	Surface temperature (K)	υ_f	Kinematic viscosity of base fluid $\left(m^2 s{-}1\right)$
k_f	Thermal conductivity of base fluid $\left(Wm^{-1}K^{-1}\right)$	k_{hnf}	Thermal conductivity of HNF $\left(Wm^{-1}K^{-1}\right)$
ρ_{hnf}	Density of HNF $\left(kgm^{-3}\right)$	σ	Electrical conductivity of base fluid (S/m)
ϕ_1, ϕ_2	Nanoparticles volume friction	Sc	Schmidth number
k_1	Porosity Parameter	M	Magnetic parameter
F_1	Inertial parameter	Pr	Prandtl number
δ	Ratio of Diffusion Cosfficient	K	Strength of homogeneous
N_T	Thermophoresis parameter	Nu	Nusselt number
N_b	Brownian motion parameter	Sh	Sherwood number
K_s	Strength of hetrogeneous	C_f	Skin friction
Ec	Eckert number	Φ	Dimensionless concentration
f'	Dimensionless velocity	θ	Dimensionless temperature
ODEs	Ordinary differential equations	HNPs	Hybrid nanoparticles
PDEs	Partial differential equations	HAM	Homotopy Analysis Method
HNF	Hybrid nanofluid	NF	Nanofluid
BL	Boundary layer		

References

1. Choi, S.U., 1995. Enhancing thermal conductivity of fluids with nanoparticles, developments and applications of non-Newtonian flows. *ASME*, FED, MD, 1995, 231, pp.99-I05.
2. Xuan, Y. and Roetzel, W., 2000. Conceptions for heat transfer correlation of nanofluids. *International Journal of heat and Mass transfer*, *43*(19), pp.3701-3707.
3. Buongiorno, J., 2006. Convective transport in nanofluids.
4. Dharmalingam, R., Sivagnanaprabhu, K.K. and Thirumalai, R., 2014. Nano materials and nanofluids: an innovative technology study for new paradigms for technology enhancement. *Procedia Engineering*, *97*, pp.1434-1441.
5. Tielke, J., Maas, M., Castillo, M., Rezwan, K. and Avila, M., 2021. Statistical analysis of thermal conductivity experimentally measured in water-based nanofluids. *Proceedings of the Royal Society A*, *477*(2250), p.20210222.
6. Coccia, G., Tomassetti, S. and Di Nicola, G., 2021. Thermal conductivity of nanofluids: A review of the existing correlations and a scaled semi-empirical equation. *Renewable and Sustainable Energy Reviews*, *151*, p.111573.
7. Alami, A.H., Ramadan, M., Tawalbeh, M., Haridy, S., Al Abdulla, S., Aljaghoub, H., Ayoub, M., Alashkar, A., Abdelkareem, M.A. and Olabi, A.G., 2023. A critical insight on nanofluids for heat transfer enhancement. *Scientific Reports*, *13*(1), p.15303.
8. Eswara Rao, M., Siva Sankari, M., Nagalakshmi, C. and Rajkumar, S., 2023. On the Role of Bioconvection and Activation Energy for MHD-Stretched Flow of Williamson and Casson Nanofluid Transportation across a Porous Medium Past a Permeable Sheet. *Journal of Nanomaterials*, *2023*.
9. Alahmadi, R.A., Raza, J., Mushtaq, T., Abdelmohsen, S.A., R. Gorji, M. and Hassan, A.M., 2023. Optimization of MHD Flow of Radiative Micropolar Nanofluid in a Channel by RSM: Sensitivity Analysis. *Mathematics*, *11*(4), p.939.
10. Ali, A., Khan, H.S., Saleem, S. and Hussan, M., 2022. EMHD nanofluid flow with radiation and variable heat flux effects along a slandering stretching sheet. *Nanomaterials*, *12*(21), p.3872.
11. Jawad, M., Shah, Z., Islam, S., Bonyah, E. and Khan, A.Z., 2018. Darcy-Forchheimer flow of MHD nanofluid thin film flow with Joule dissipation and Navier's partial slip. *Journal of Physics Communications*, *2*(11), p.115014.
12. Jawad M, Saeed A, Khan A, Islam S. MHD bioconvection Darcy-Forchheimer flow of Casson nanofluid over a rotating disk with entropy optimization. Heat Transfer. 2021 May;50(3):2168-96.

 doi:10.20944/preprints202405.1553.v1

13. Jawad, M., Saeed, A., Kumam, P., Shah, Z. and Khan, A., 2021. Analysis of boundary layer MHD Darcy-Forchheimer radiative nanofluid flow with soret and dufour effects by means of marangoni convection. *Case Studies in Thermal Engineering*, *23*, p.100792.
14. Roşca, N.C., Roşca, A.V., Aly, E.H. and Pop, I., 2021. Flow and heat transfer past a stretching/shrinking sheet using modified Buongiorno nanoliquid model. *Mathematics*, *9*(23), p.3047.
15. Hayat, T. and Nadeem, S., 2017. Heat transfer enhancement with Ag–CuO/water hybrid nanofluid. *Results in physics*, *7*, pp.2317-2324.
16. Waini, I., Ishak, A. and Pop, I., 2019, November. Hybrid nanofluid flow and heat transfer past a permeable stretching/shrinking surface with a convective boundary condition. In *Journal of Physics: Conference Series* (Vol. 1366, No. 1, p. 012022). IOP Publishing.
17. El-Zahar, E.R., Rashad, A.M., Saad, W. and Seddek, L.F., 2020. Magneto-hybrid nanofluids flow via mixed convection past a radiative circular cylinder. *Scientific Reports*, *10*(1), p.10494.
18. Rasheed, T., Hussain, T., Anwar, M.T., Ali, J., Rizwan, K., Bilal, M., Alshammari, F.H., Alwadai, N. and Almuslem, A.S., 2021. Hybrid nanofluids as renewable and sustainable colloidal suspensions for potential photovoltaic/thermal and solar energy applications. *Frontiers in Chemistry*, *9*, p.737033.
19. Waini, I., Jamaludin, A., Nazar, R. and Pop, I., 2022. MHD flow and heat transfer of a hybrid nanofluid past a nonlinear surface stretching/shrinking with effects of thermal radiation and suction. *Chinese Journal of Physics*, *79*, pp.13-27.
20. Nadeem, M., Siddique, I., Awrejcewicz, J. and Bilal, M., 2022. Numerical analysis of a second-grade fuzzy hybrid nanofluid flow and heat transfer over a permeable stretching/shrinking sheet. *Scientific Reports*, *12*(1), p.1631.
21. Sarfraz, M., Yasir, M. and Khan, M., 2023. Multiple solutions for non-linear radiative mixed convective hybrid nanofluid flow over an exponentially shrinking surface. *Scientific Reports*, *13*(1), p.3443.
22. Jawad, M., Khan, Z., Bonyah, E. and Jan, R., 2022. Analysis of hybrid nanofluid stagnation point flow over a stretching surface with melting heat transfer. *Mathematical Problems in Engineering*, *2022*.
23. Jawad, M., Khan, A. and Shah, S.A.A., 2021. Examination of couple stress hybrid nanoparticles (CuO-Cu/blood) as a targeted drug carrier with magnetic effects through porous sheet. *Brazilian Journal of Physics*, *51*(4), pp.1096-1107.
24. Jawad, M., Saeed, A., Tassaddiq, A., Khan, A., Gul, T., Kumam, P. and Shah, Z., 2021. Insight into the dynamics of second grade hybrid radiative nanofluid flow within the boundary layer subject to Lorentz force. *Scientific Reports*, *11*(1), p.4894.
25. Waini, I., Ishak, A. and Pop, I., 2021. Hybrid Nanofluid Flow with Homogeneous-Heterogeneous Reactions. *Computers, Materials & Continua*, *68*(3).
26. Xu, N.L., Xu, H. and Raees, A., 2018. Homogeneous-heterogeneous reactions in flow of nanofluids near the stagnation region of a plane surface: The Buongiorno's model. *International Journal of Heat and Mass Transfer*, *125*, pp.604-609.
27. Alarabi, T.H., Rashad, A.M. and Mahdy, A., 2021. Homogeneous–heterogeneous chemical reactions of radiation hybrid nanofluid flow on a cylinder with joule heating: Nanoparticles shape impact. *Coatings*, *11*(12), p.1490.
28. Ramzan, M., Chaudhry, H., Ghazwani, H.A.S., Kadry, S., Shahmir, N., Abbas, M. and Saleel, C.A., 2023. Impact of homogeneous–heterogeneous reactions on nanofluid flow through a porous channel–A Tiwari and Das model application. *Numerical Heat Transfer, Part A: Applications*, pp.1-14.
29. Anuar NS, Bachok N, Pop I. Cu-Al2O3/water hybrid nanofluid stagnation point flow past MHD stretching/shrinking sheet in presence of homogeneous-heterogeneous and convective boundary conditions. Mathematics. 2020 Jul 28;8(8):1237.
30. Bala Anki Reddy, P., Suneetha, S., Subbarayudu, K., Al-Arabi, T.H. and Rashad, A.M., 2021. Exploration of physical features of homogeneous–heterogeneous chemical action in a nanofluid film dispensed with MOS2 in diathermic oils. *Journal of Taibah University for Science*, *15*(1), pp.826-839.
31. Khashi'ie, N.S., Arifin, N.M. and Pop, I., 2022. Magnetohydrodynamics (MHD) boundary layer flow of hybrid nanofluid over a moving plate with Joule heating. *Alexandria Engineering Journal*, *61*(3), pp.1938-1945.
32. Reddy, Y.D., Goud, B.S., Nisar, K.S., Alshahrani, B., Mahmoud, M. and Park, C., 2023. Heat absorption/generation effect on MHD heat transfer fluid flow along a stretching cylinder with a porous medium. *Alexandria Engineering Journal*, *64*, pp.659-666.
33. Abbas, N., Shatanawi, W., Shatnawi, T.A. and Hasan, F., 2023. Theoretical analysis of induced MHD Sutterby fluid flow with variable thermal conductivity and thermal slip over a stretching cylinder. *AIMS Mathematics*, *8*(5), pp.10146-10159.
34. Rashad, A.M., Nafe, M.A. and Eisa, D.A., 2023. Heat variation on MHD Williamson hybrid nanofluid flow with convective boundary condition and Ohmic heating in a porous material. *Scientific Reports*, *13*(1), p.6071.

 doi:10.20944/preprints202405.1553.v1

35. Suresh Kumar, Y., Hussain, S., Raghunath, K., Ali, F., Guedri, K., Eldin, S.M. and Khan, M.I., 2023. Numerical analysis of magnetohydrodynamics Casson nanofluid flow with activation energy, Hall current and thermal radiation. *Scientific Reports*, *13*(1), p.4021.